ACS OMEGA

http://pubs.acs.org/journal/acsodf

Article

Investigations on Crystalline Perfection, Raman Spectra and Optical Characteristics of Transition Metal (Ru) Co-Doped Mg:$LiNbO_3$ Single Crystals

M. K. Raseel Rahman, B. Riscob, Rajeev Bhatt, Indranil Bhaumik, Sarveswaran Ganesamoorthy, Narayanasamy Vijayan, Godavarthi Bhagavannarayana, Ashwini Kumar Karnal, and Lekha Nair*

Cite This: *ACS Omega* 2021, 6, 10807−10815

Read Online

ACCESS | Metrics & More | Article Recommendations

ABSTRACT: Congruent lithium niobate single crystals with a Ru:Mg co-dopant have been successfully grown using the Czochralski technique from the melt containing 0.02 mol % Ru with Mg of two varied concentrations (4.0 and 6.0 mol %). The effects of Ru and Mg co-doping on the crystalline quality were determined by high-resolution X-ray diffractometry, which confirmed that the crystalline quality is good and that the dopants are statistically distributed in the crystal. The Raman scattering analysis shows no change in the lattice vibration except a slight change in the peak width and intensity due to more asymmetry in the molecular charge, which leads to enhancement of the polarizability. The optical transmission spectra indicate that both the crystals have high optical transparency in the visible region, with a shift of the absorption edge toward shorter wavelengths, as compared to un-doped LN. The weak absorption band observed below 400 nm is attributed to Ru ions. The influence of co-doping in the electronic band gap energies is calculated by the Tauc relation. The refractive index is measured by using a prism coupler at two wavelengths (532 and 1064 nm). The calculated absorption coefficients and direct and indirect band gap energies for both the samples are found to be nearly the same within experimental error. A decrease in the birefringence is observed for the Ru:Mg(6 mol %) doped sample. The observed slight reduction in refractive indices with Ru:Mg co-doping is consistent with a rise in band gap energy, which is related to the change in absorption edge to the lower wavelength. The second harmonic generation (SHG) efficiency is measured by the Kurtz and Perry powder method, and a decrease in SHG efficiency for Ru:Mg(6 mol %) is observed.

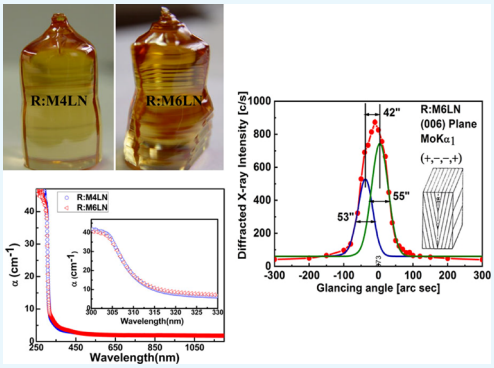

INTRODUCTION

The lithium niobate ($LiNbO_3$, LN) single crystal, also called the "silicon of photonics",[1] is the most important optical material that has been used in a wide range of applications in photonics like optical modulators, optical waveguides, optical frequency conversion, optical parametric oscillators (OPOs), holographic data storage, and wavelength and surface acoustic wave (SAW) filters. This versatility is due to a remarkable combination of excellent nonlinear optical (NLO), electro-optical (EO), photorefractive, ferroelectric, and wave guiding properties.[2−4] Since the first growth of LN reported in 1965,[5] LN has continued to be studied extensively with investigations on new dopants and modifications in growth conditions,[6] resulting in its widespread use in different applications.[7,8]

Physical properties of LN are highly dependent on the [Li]/[Nb] ratio. LN can be grown in near-stoichiometric (off-congruent) and nonstoichiometric (congruent) forms depending upon the [Li]/[Nb] cation ratio.[9,10] Congruent LN (Li/Nb ∼0.946, CLN) crystals are more widely used for applications due to their compositional stability during growth. It is well known that CLN presents a large concentration of intrinsic defects and disorder in the crystallographic frame such as an excess of Nb antisite defects (Nb_{Li}^{5+}) and Li cation vacancies (V_{Li}^{-1}).[11] The presence of such defects restricts many of the optical applications. Physical properties and device performance of LN can be optimized by doping with suitable ions in the crystallographic lattice within a threshold limit concentration. The selection of the type and amount of dopant are also very important because they offer a wide range of variations in responses. Different types of dopants have been used for various applications of the LN crystals such as Mg, Zn, In, and Zr for suppressing the optical damage and metal ions

Received: January 25, 2021
Accepted: March 26, 2021
Published: April 15, 2021

like Fe, Mn, Cu, Ce, and Ru to improve photorefractive properties.[12−14]

One of the key issues in LN is the observance of optical damage (beam distortion) upon exposure to intense visible laser radiation, which occurs as a result of the creation of refractive index changes in LN that limit its practical applications in nonlinear optics and electro-optics, and several research efforts have been focused on this.

Zhong *et al.*[15] observed that LN with a 4.6 or higher mol% of Mg added to the melt can lead to strongly enhanced optical damage resistance, to about 100 times as large as that of the undoped crystals, which was later confirmed by Bryan *et al.*[16] From then on, Mg-doped crystals have been extensively studied, applied, and reported in the literature like growth,[17−19] phase equilibrium,[18] defect structures, which are widely studied in accordance with the Li site vacancy model,[20,21] characterization, and properties.[22−26] Hence, for a long time now, Mg:LN is being used in optical parametric oscillation, terahertz generation, and optical waveguides.

Ruthenium (Ru), a transition metal, close to iron (Fe) in the periodic table, exists in different valence states in the grown crystal. In the three valence states of Ru^{3+}, Ru^{4+}, Ru^{5+},[27] Ru ions have different energy levels in the crystals. Due to the closeness of Ru with Fe, it is assumed that the doping effect of Ru in nonlinear crystals would be similar. The Ru-ion doping in NLO crystals has been studied, such as in Ru:$LiNbO_3$,[28] Ru:$Bi_{12}SiO_{20}$,[27] Ru:$Bi_4Ge_3O_{12}$,[29] Ru:$Sr_{0.61}Ba_{0.39}Nb_2O_6$,[30] and Ru:$Bi_{12}TiO_{20}$.[31] Like Fe, Ru-ion doping in LN may be supportive to improve the photorefractive characteristics. It is important to note that keeping the homogeneity of Ru content in the LN crystal is a challenge because the effective segregation coefficient of Ru is greater than 1 and evaporation of Ru takes place during growth.[32] It was found that Ru content in LN slowly decreases along the pulling direction, and extra care has to be taken for the growth of the doped single crystals.

In the present investigation, the above consideration is kept in mind, and single crystals of undoped congruent LN and Ru:Mg co-doped congruent LN, i.e., Ru(0.02 mol %):Mg(4.0 mol %)_CLN and Ru(0.02 mol %):Mg(6.0 mol %)_CLN (hereafter termed as CLN, R:M4LN, R:M6LN, respectively), have been grown by using the Czochralski (Cz) method. Crystalline perfection was studied by high-resolution X-ray diffraction. The effects of structural disorder on the vibrational modes of doped crystals were analyzed by Raman spectra. The optical transmission spectra in the UV−vis and the near-IR regions were measured to study the effect of dopants on optical absorption, defect structures, and the band gap of the crystal. The refractive indices were measured at two wavelengths (532 and 1064 nm) to evaluate the effect of Ru:Mg doping on the birefringence of LN single crystals. The SHG properties were measured by the Kurtz and Perry powder method.

EXPERIMENTAL SECTION

Crystal Growth. LN powders were synthesized from high-purity (99.999%) raw materials Li_2CO_3 and Nb_2O_5 weighed according to the congruent ratio (Li/Nb = 48.46:51.54). For Ru:Mg co-doped crystals, a fixed concentration of RuO_2 (0.02 mol %) and different concentrations of MgO, i.e., 4.0 and 6.0 mol %, were used. The raw materials were mixed thoroughly by the ball milling process in a Turbula 3D shaker mixer in ethyl alcohol and dried. The synthesis was carried out by solid-state reaction at 1174 K for 24 h.[33] The mixed precursors were heated from room temperature to the reaction temperature at a slow rate of 80 K/h with an intermediate dwelling at 900 K for 5 h to allow slow and nonviolent decomposition of lithium carbonate. Then, the RuO_2 (99.99%) powders were added to the calcined mixtures. Prior to synthesis, the mixtures were mixed once again and transferred to a platinum crucible (50 mm height and 50 mm diameter). Single crystals of R:M4LN and R:M6LN were grown by using a Cyberstar Czochralski crystal puller attached with a Huttinger Induction Heating system (8 kHz, 50 kW). The growth temperature and post-cooling rate were controlled by using a Eurotherm (902) PID temperature controller. A good quality *Z* cut seed crystal was used. The rotation and pulling rates were ∼5−25 r min^{-1} and 5 mm h^{-1}, respectively. After the growth, the cooling rate was maintained at 20 K h^{-1} across phase transition temperature (1423 K) and then the cooling rate was increased to room temperature. The grown crystals were yellow-red-colored, with a size of 30 mm in length, 25 mm in diameter, and crack-free (Figure 1). The grown crystals were cut into wafers, well-polished, and subjected to various characterization techniques.

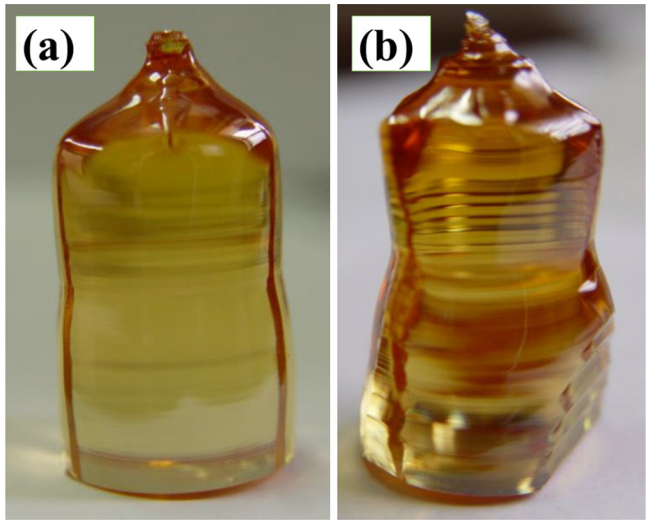

Figure 1. Photograph of the Czochralski-grown (a) R:M4LN and (b) R:M6LN crystals.

High-Resolution X-ray Diffractometry. The crystalline perfection of the as-grown Ru:Mg co-doped LN crystals was assessed by high-resolution diffraction curves recorded by using a multicrystal X-ray diffractometer (MCD) developed at NPL, Delhi.[34] The details of the HRXRD measurement are given elsewhere.[35,36]

Raman Spectroscopy. Raman spectra were recorded on a [001] single-crystal wafer using a HORIBA-T64000 Triple Raman spectrometer equipped with a 514.5 nm Ar^+-ion laser (Spectra-Physics) as an excitation source, having a beam power of 80 mW. The spectra were measured at room temperature in the wavenumber range of 100−1000 cm^{-1}.

UV−vis−NIR Spectroscopy. The optical absorption and transmission spectra were examined by using a Jasco V-263 spectrophotometer in the UV−vis−NIR region. The measurements were carried out at room temperature with unpolarized light at normal incidence. 1 mm-thick finely polished crystal samples were used.

Conoscopy Study. The homogeneity of Ru:Mg co-doped crystals was examined under crossed polarization conditions by

https://doi.org/10.1021/acsomega.1c00452
ACS Omega 2021, 6, 10807−10815

a Conoscopy study with an OLYMPUS BX-60 polarized light optical microscope. The [001] oriented optically polished crystal samples were used for the measurement.

Refractive Index Measurement. A Prism coupler (model 2010/M; Metricon Corporation, UK) was used to measure the refractive index for the present samples. A *z*-cut polished plate of thickness 1 mm was used for this measurement. The details of the refractive index measurement are given elsewhere.[37]

SHG Measurement. The SHG behaviors of the grown crystals were examined by the Kurtz and Perry powder technique[38] using potassium dihydrogen phosphate (KDP) as standard reference. The crystals were powdered to a particle size of ∼125−150 μm, and the resultant homogeneous powder was densely filled in a microcapillary tube of uniform bore and exposed to laser radiation. A Nd:YAG laser (λ = 1064 nm, input beam energy of 4.7 mJ/pulse, repetition rate of 10 Hz, and pulse width of 8 ns) was used as a source. The SHG signal generated from the randomly oriented microcrystal was collected by a lens and detected by a photomultiplier tube.

RESULTS AND DISCUSSION

High-Resolution XRD Analysis. To study the effect of Ru:Mg co-doping on the crystalline perfection of as-grown undoped and doped single crystals, the high-resolution X-ray diffraction (HRXRD) curves (DCs) were recorded under identical measurement conditions (same X-ray power, beam height, and beam width) for the (006) diffraction planes of the undoped and doped LN crystals using Mo Kα_1 radiation in symmetrical Bragg geometry. The DCs for the CLN, R:M4LN, and R:M6LN single crystals are shown in Figure 2a−c, respectively. The DC of the undoped LN single crystals (Figure 2a) shows a single peak with nearly perfect symmetry with respect to its center. The absence of an additional satellite peak with symmetry indicates that the crystalline perfection is nearly perfect and is free from cracks, twins, and internal structural grain boundaries though the probability of formation of cracks and boundaries in LN is common due to the structural phase transition with a volume change during the cooling cycle of LN crystal growth.[39,40] The symmetric (with respect to the diffraction peak position taken as zero), sharp DC for the CLN (Figure 2a) having a full width at half-maximum (FWHM) of 29 arc sec is as expected for a perfect crystal, which is however more than the theoretically calculated value for an ideally perfect crystal from the plane wave theory of dynamical X-ray diffraction,[41] i.e., 2.6 arc sec,[42] but is comparable with the experimentally reported value of 21 arc sec for CLN[43] and is also very common in real-life crystals.[36] The comparatively higher value of FWHM for pure LN specifies the existence of some point defects and their aggregates, which are unavoidable and inevitably arise during the crystal growth.

There are some interesting features in the diffraction curves of doped crystals. As evident from the curve in Figure 2b, the DC for R:M4LN has a single peak having an FWHM of 67 arc sec with asymmetry with respect to the peak position of the curve. The FWHM of this DC is considerably larger than the value of pristine LN. The asymmetry and the broadening of the DC reveal that the Ru:Mg co-doping leads to enhancement of point defects in the LN crystal lattice. The diffraction intensity at a higher glancing angle (θ) with respect to the peak position, i.e., in the positive side, is more than that in the negative side. This feature indicates that the crystal structure contains a predominantly interstitial type of point defect and shows the

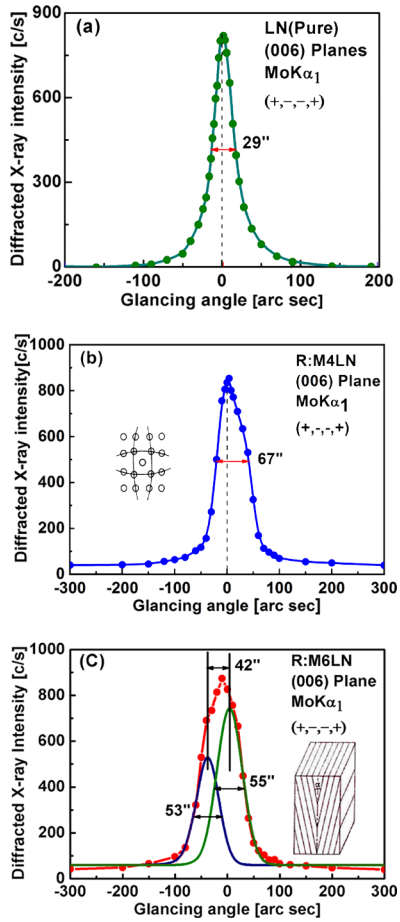

Figure 2. DCs for LN single crystals using the (006) diffracting planes with Mo Kα_1 radiation and recorded under identical conditions. The curves in panels (a), (b), and (c), respectively, belong to CLN, R:M4LN, and R:M6LN.

capability of the lattice to accommodate the Ru:Mg dopants.[44] According to the Bragg equation ($n\lambda = 2d \sin \theta_B$, where d is the interplanar distance, n is the order of reflection, λ is the wavelength of the X-ray used, and θ_B is the Bragg angle), θ_B and d are inversely proportional. The inset in the DC shows how the lattice undergoes a change around the point defect core. The interplanar spacing, d, around the very defect core and hence the lattice around the defect core has undergone compressive stress[44] leading to more scattering at the slightly higher (positive side) Bragg angles.

Figure 2c shows the DC for the R:M6LN crystal with much more broadening. On careful observation, the curve is not depicting a single peak. On deconvolution of the diffraction curves, it is clear that the DC contains two peaks instead of a single peak. The solid curve, which is well fitted with the experimental points (filled circles), is the convoluted curve of the two peaks. The additional peak depicts an internal structural with a very low angle (tilt angle ≤1 arc min) grain boundary[39] whose tilt angle (α = misorientation angle between the two crystalline regions on both sides of the structural grain boundary as shown in the inset) is 42 arc sec from the main crystalline block. The FWHM (full width at half-maximum) of the main peak and the very low angle boundaries are, respectively, 55 and 53 arc sec, which are higher as expected for the doped crystals. At higher concentration of dopants, the crystal has undergone some internal stress and finally leads to

https://doi.org/10.1021/acsomega.1c00452
ACS Omega 2021, 6, 10807−10815

the formation of a very low angle boundary. However, the FWHMs of the DCs of the two crystalline regions are not high signifying that the crystalline perfection of the two crystalline regions on both sides of the low angle boundary is reasonably good. It is worth mentioning here that such very low angle boundaries could be detected because of the high resolution of the in-house developed multicrystal X-ray diffractometer used in the present study.[34]

The above analysis indicates that in comparison to the undoped LN, the Ru and Mg ions are more or less uniformly accommodated in the crystal lattice. If the dopants are randomly accommodated as macroscopic clusters, then the strain generated due to such clusters will lead to structural subgrain boundaries with tilt angles in arc minutes or even in arc degrees and finally lead to cracks in the case of doped crystals at high concentrations.[6] Here, such macroscopic defects are absent in the grown undoped as well as doped crystals. The good amount of scattered intensity along the tails on both sides of the DC of doped crystals also confirms the fact that in addition to the interstitial occupation of some dopants in the lattice, Ru and Mg ions occupied the substitutional sites of Li^{+} and Nb^{5+} leaving some Li vacancies.

The integrated intensity, i.e., the total area under the curve (ρ) of the DC, is another interesting parameter to assess the degree of crystalline perfection.[35] No real crystal could be either ideally perfect or ideally mosaic. The measured ratio between the integrated intensity of undoped LN, R:M4LN, and R:M6LN is 1:1.6:2.1, which indicates that in the doped crystals the dopants are statistically distributed in the crystal lattice and are not agglomerated into mosaic blocks.

Raman Analysis. Raman scattering also gives important information about the structural perfection of the crystals, i.e., deformation of the lattice and the presence of point defects in the crystal structure.[45] Different peaks in the Raman spectra correspond to different vibrational modes. Figure 3 shows the

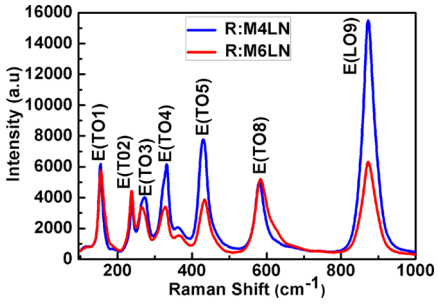

Figure 3. Raman spectra of the R:M4LN and R:M6LN single crystals measured along the Z(YX)Z scattering configuration.

recorded Raman spectra of R:M4LN and R:M6LN obtained from the wafer taken from the middle of the grown crystals. The measurements are recorded in the Z(YX)Z configuration. The E(TO1) mode at a wavenumber of 154 cm^{-1} is attributed to Nb−O vibrations. The peak at 365 cm^{-1} is the E(TO6) mode, which corresponds to Li−O vibration. The peak at 580 cm^{-1} is the E(TO8) mode, attributed to the stretching vibration of the oxygen octahedron.[46,47] There is no variation in the wavenumber of the Raman peaks when the crystal is doped with Ru and Mg. The full width at half-maximum (FWHM) of the Raman peaks is related to the presence of disorder in the crystal lattice structure. There is no shift in the peak position except the variation in peak intensities and FWHM, which show that there is no structural change except for the change in point defect concentration, which is in line with the observed HRXRD results. The strong peak at 872 cm^{-1} is attributed to LO modes of the Li sublattice, and the line-width of the same is correlated to the Li content in the lattice. The FWHMs of the 872 cm^{-1} peaks for the R:M4LN and R:M6LN samples are 38.25 and 44.43, respectively. The increase in FWHM of the peaks with the increase of Mg indicates the increase in disorder within the crystal structure. This is in good agreement with HRXRD data depicting higher FWHM for R:M6LN due to increased structural disorder because of additional Mg ions in comparison with that of R:M4LN. The change in FWHM for E(TO1) at 154 cm^{-1} and E(TO7) at 433 cm^{-1} may be due to the fact that the addition of Mg ions makes the disorder in the Nb sublattice and Li sublattice, respectively. It is known that initially Ru and Mg ions replace the Nb cations at the Li site whereas a further increase of Mg gradually replaces Li from its site, leaving some Li vacancies due to charge imbalance.

The presence of concentration of lithium (C_{Li}) in the crystals can be analyzed by using the LO modes at 872 cm^{-1} by using the formula[48]

$$(C_{Li}) = 53.29 - 0.1837\Gamma\ [cm^{-1}] \quad (1)$$

where Γ stands for the FWHM of the peak at a particular position. The calculated values for R:M4LN and R:M6LN are 47.98 and 47.12 mol %, respectively, which shows that co-doping might replace Li in the lattice.

UV−vis−NIR Analysis. Optical transparency was measured on fine polished 1 mm-thick Ru:Mg-doped LN crystal wafers cut along the growth direction (z-direction). Figure 4a shows the recorded transmission spectra of R:M4LN and R:M6LN in the wavelength range of 200−1200 nm. The obtained spectra show that both the crystals exhibit high optical transparency in the visible region. Further, the absorption coefficient (α) was calculated from the transmittance spectra measured at room temperature using the following relation[49]

$$T \approx (1 - R)^2 \exp(-\propto d) \quad (2)$$

where T is the transmittance, R is the reflectivity (calculated from refractive index (n) determined from Sellmeier's equation using the relation $R \sim (n-1)^2/(n+1)^2$ to account for the Fresnel reflection loss), and d is the sample thickness. The refractive index (n) was calculated from Sellmeier's dispersion relation reported in the literature.[50]

The absorption coefficient ($\propto$) spectra of both the crystals are shown in Figure 4b. The absorption edge (AE) is considered as the position of the wavelength where the absorption coefficient is 20 cm^{-1}.[51] The measured AEs of the R:M4LN and R:M6LN crystals are both 309 nm; the AE shifts toward a lower wavelength in comparison to 320 nm for undoped LN.[52] As LN contains Nb antisite defects and Li vacancies, this observation suggests that the co-doping of Ru:Mg improves the optical band structure, which is due to lowering of intrinsic structural defects ($Nb_{Li}^{5+}$and V_{Li}^{-1}) in the grown crystals as discussed earlier. Further, a very weak absorption below 400 nm can be seen in the absorption and transmission spectra. This may be attributed to structural defects associated with Ru ions in the Mg:LN crystal as Ru ions exhibit absorption peaks around 370 and 530 nm.[53]

https://doi.org/10.1021/acsomega.1c00452
ACS Omega 2021, 6, 10807−10815

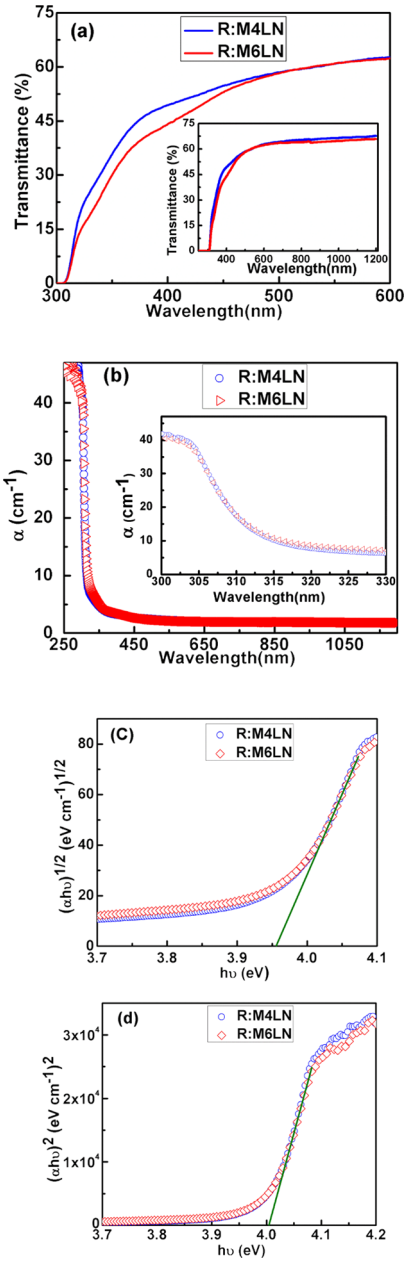

Figure 4. (a) Optical transmission spectra, (b) absorption coefficient spectra, (c) direct band gaps, and (d) indirect band gaps of R:M4LN and R:M6LN.

Further, the effects of Ru:Mg co-doping on the electronic band gap energies of LN are calculated by using the Tauc relation[54]

$$\alpha h\upsilon \propto (h\upsilon - E_g)^n \tag{3}$$

where $h\upsilon$ is the photon energy, E_g is the allowed energy gap, and n is an exponent determined by the nature of the electronic transition during the absorption process. The value $n=\frac{1}{2}$ is for the allowed direct transition, and $n = 2$ is for the allowed indirect transition. Figure 4c shows the plot of $(\alpha h\upsilon)^{1/2}$ versus $h\upsilon$ for the R:M4LN and R:M6LN crystal samples. The intercept with the energy axis (at $\alpha = 0$) of the straight-line fit from the linear region of the plot provides the indirect band gap energy (E_g^{ind}). The observed optical indirect band gap energy value is the same for both the samples, which is 3.95 eV. The plot of $(\alpha h\upsilon)^2$ versus $h\upsilon$ (Figure 4d) gives the information for the direct band gap transition. The straight line from the step rise of absorption at the higher photon energy intercept with the energy axis ($\alpha = 0$) gives the direct band gap energy (E_g^d), which is 4.0 eV for both R:M4LN and R:M6LN. The observed indirect and direct band gap energies for the R:M4LN and R:M6LN samples are higher than the band gap energies of the CLN crystal.[55] The values of AE and the direct and indirect band gap energies are summarized in Table 1. The

Table 1. Direct and Indirect Band Gap Energies of Different Samples along with Absorption Edges (AEs) and Urbach Energies

Sample	AE (nm)	E_g^d (eV)	E_g^{ind} (eV)	E_u (meV)
CLN[a]	318	3.93	3.77	78
R_M4:CLN	308	4.00	3.95	117
R_M6:CLN	308	4.00	3.95	117

[a]Ref 55.

increase in band gap energies of doped samples confirms reduction of structural defects. The increase in the band gap due to Ru:Mg doping is related to the shift in absorption edge toward the lower wavelength.

Further, the Urbach behavior of the absorption edge in crystalline and amorphous materials characterizes the lattice disordering of the material. The exponential increase of the absorption coefficient with incident photon energy gives an Urbach tail, which gives information on the energy width of localized states and the presence of different types of disorders and intrinsic defects in the energy band gap. The exponential character of the absorption coefficient near the fundamental AE is expressed by the following empirical relation[56]

$$\alpha = \alpha_0 \exp(h\upsilon/E_u) \tag{4}$$

where α_0 is a characteristic crystal parameter and E_u is the Urbach energy, which corresponds to the width of defect tail states. E_u is calculated from the reciprocal of the slope of the linear fit of the $\ln(\alpha)$ versus $h\upsilon$ plot (Figure 5)

$$E_u^{-1} = \frac{\Delta(\ln \alpha)}{\Delta(h\upsilon)} \tag{5}$$

The calculated Urbach energy for R:M4LN and R:M6LN are the same, which is 117 meV. The high value of Urbach energy for the Ru:Mg-doped crystal with respect to undoped LN (78 meV)[55] indicates that the doped crystals may contain additional point defects like F-centers and oxygen vacancies apart from intrinsic defects or doping-induced structural

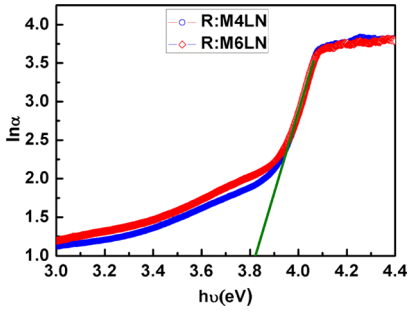

Figure 5. Dependence of the logarithm of the absorption coefficient $\ln(\alpha)$ with incident photo energy.

https://doi.org/10.1021/acsomega.1c00452
ACS Omega 2021, 6, 10807−10815

disorder. This is also consistent with the observation in the HRXRD measurements in which the higher FWHM is observed for the doped crystal in comparison to CLN.

Refractive Index and Birefringence Analysis. The extraordinary (n_e) and ordinary (n_o) refractive indexes of the as-grown CLN, R:M4LN, and R:M6LN crystals have been measured and plotted for two wavelengths, 532 and 1064 nm, at room temperature. The measurement is carried out by using the prism coupler technique.[37] The error was estimated as described in ref 34. In comparison to the undoped LN, both n_o and n_e for 532 nm are gradually decreasing (Figure 6a) with

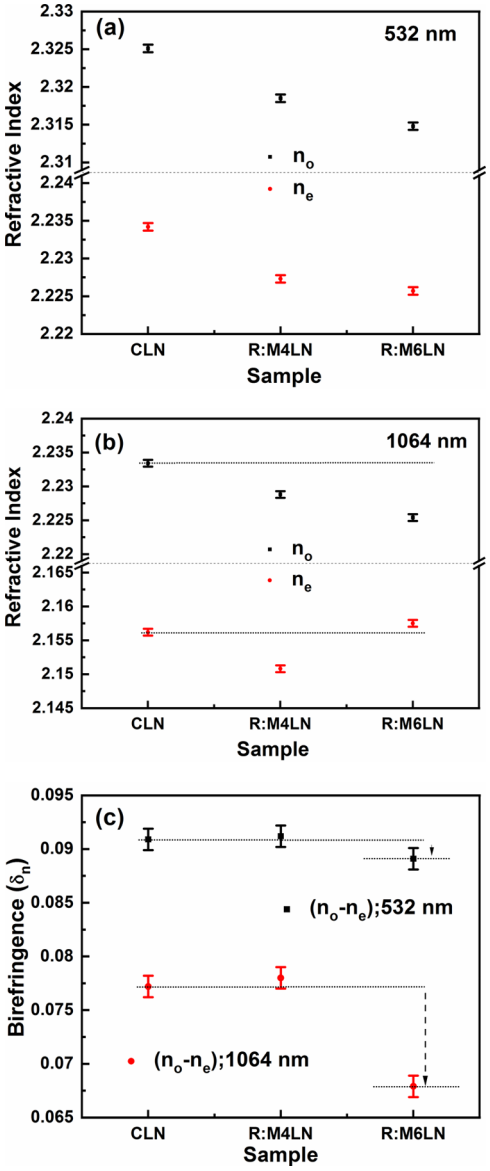

Figure 6. Refractive indexes of the undoped, R:M4LN, and R:M6LN single crystals at (a) 532 and (b) 1064 nm. (c) Birefringence of undoped, R:M4LN, and R:M6LN.

the increase of Ru:Mg doping concentration. From Figure 6b, it is evident that at 1064 nm, n_o decreases with the increase in Ru:Mg dopant concentration, but n_e is slightly higher for R:M6LN than for R:M4LN and is nearly the same as that of undoped LN. The observed reduction in the refractive index of R:M4LN at both the wavelengths may be due to the modification in the defect structure, particularly the decrease in intrinsic defects (Nb_{Li}^{5+} and V_{Li}^{-1}) due to Ru:Mg doping. δ_n is the birefringence, defined as $\delta_n = n_o - n_e$. In contrast to undoped LN, δ_n increases for R:M4LN, whereas it decreases for R:M6LN at both the wavelengths, 532 and 1064 nm. The comparatively higher birefringence for R:M4LN is suitable for photonic applications. The refractive index and band gap energy are related by the relation $n^2 \simeq 1 + C/E_g$,[57] where C is a material constant. The observed slight decrease in the refractive indices with doping is consistent with the increase in band gap energy, which is related to the shift in the absorption edge toward the lower wavelength (Table 2).

Conoscopy Patterns. The observed conoscopy patterns of the c-cut plates of the R:M4LN and R:M6LN samples under a polarized light optical microscope in transmission mode are shown in Figure 7a,b, respectively. The observed conoscopy patterns are nearly well shaped and symmetrical. The symmetrical fringe patterns show good compositional and hence good optical homogeneity, which shows that the doped crystals are free from residual stress. A retarder plate (532 nm) is inserted in the optical path, and the interference pattern is examined to see the influence of dopants on the birefringence behavior and mainly on the optic sign of the crystal. The blue color appearance in the second and fourth quadrants confirms the negative optical sign of the grown crystals. It is therefore confirmed that doped lithium niobate crystals are negative uniaxial and doping (Mg, Ru) does not influence its optic sign.

SHG Analysis. The SHG properties of the undoped and Ru:Mg doped LN samples were confirmed by the green light (532 nm) at the output during powder SHG measurement. Table 3 gives the output power values of the CLN, R:M4LN, and R:M6LN samples along with the output power of standard KDP. The relative SHG efficiencies of CLN, R:M4LN, and R:M6LN are 2.88, 2.91, and 2.44, respectively, compared to that of the standard KDP crystal. The NLO efficiency initially increased for the R:M4LN sample and the decreased for the R:M6LN sample where the Mg concentration is higher. This observation shows the dependence of SHG on the doping concentration as it influences the crystalline perfection. The reduction in SHG for R:M6LN may be due to the presence of low angle boundaries as observed in HRXRD studies.[35] The presence of low angle boundaries will influence the SHG due to possible phase mismatch between the fundamental and nonlinear fields associated with grain misorientation. In addition, the decrease in SHG may also be attributed to a decrease in the nonlinear optical coefficients associated with the presence of foreign ions in the crystal.[58]

CONCLUSIONS

In conclusion, high-quality Ru:Mg co-doped $LiNbO_3$ single crystals were grown from congruent melts by the Czochralski method. The HRXRD analysis confirmed that the crystalline perfection of the pure and Ru:Mg-doped crystals is good. The UV−vis−NIR spectral analysis shows that the co-doping shifts the absorption edge toward a shorter wavelength. The optical band gap energies for direct and indirect transitions were evaluated. The obtained absorption edges and direct and indirect band gap energies are the same for both Ru:Mg-doped samples. The presence of an absorption band around 400 nm in doped crystals makes them suitable for photorefractive and beam coupling applications. The well-shaped, symmetrical conoscopy patterns of doped LN confirm good compositional and hence good optical homogeneity, which shows that the

https://doi.org/10.1021/acsomega.1c00452
ACS Omega 2021, 6, 10807−10815

Table 2. Evaluated n_o, n_e, and δ_n Values of the CLN, R:M4LN, and R:M6LN Single Crystals

	at wavelength 532 nm			at wavelength 1064 nm		
crystal	n_o	n_e	δ_n	n_o	n_e	δ_n
CLN	2.3251	2.2342	0.090(9)	2.2334	2.1562	0.077(2)
R:M4LN	2.3185	2.2273	0.091(2)	2.2288	2.1508	0.078(0)
R:M6LN	2.3148	2.2257	0.089(1)	2.2254	2.1572	0.067(9)

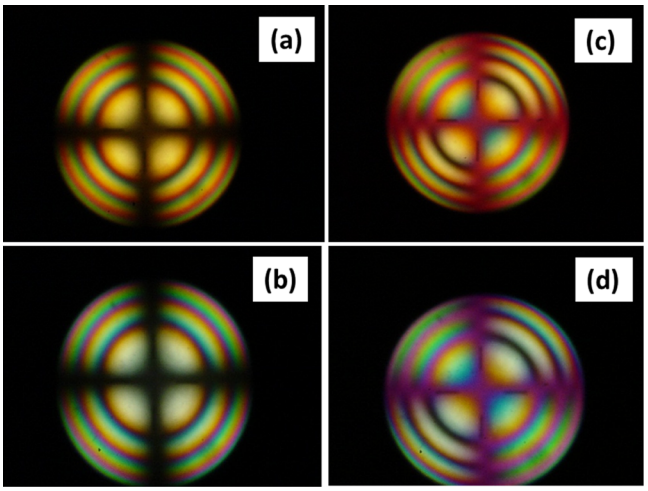

Figure 7. Conoscopic patterns for the LN crystal: (a) R:M4LN and (b) R:M6LN. Changes in the conoscopic patterns after insertion of the retarding (λ=532 nm) waveplate: (c) R:M4LN and (d) R:M6LN.

Table 3. Relative SHG Output

sample	power output
KDP	13.6 mV
CLN	39.2 mV
R:M4LN	39.6 mV
R:M6LN	29.2 mV

doped crystals are free from residual stress. The observed slight decrease in refractive indices with doping is consistent with an increase in band gap energy, which is related to the shift in the absorption edge toward the lower wavelength. The comparatively low SHG efficiency of R:M6LN may be due to the presence of low angle boundaries as observed from the crystalline perfection.

AUTHOR INFORMATION

Corresponding Author

Lekha Nair − *Department of Physics, Jamia Millia Islamia, New Delhi 110025, India;* orcid.org/0000-0002-9643-0536; Email: lnair@jmi.ac.in

Authors

M. K. Raseel Rahman − *Department of Physics, Jamia Millia Islamia, New Delhi 110025, India*

B. Riscob − *Institute for Plasma Research, Gandhinagar 382428, India*

Rajeev Bhatt − *Crystal Growth and Instrumentation Section, Laser and Functional Materials Division, Raja Ramanna Centre for Advanced Technology, Indore 452013, India; Homi Bhabha National Institute, Mumbai 400094, India*

Indranil Bhaumik − *Crystal Growth and Instrumentation Section, Laser and Functional Materials Division, Raja Ramanna Centre for Advanced Technology, Indore 452013, India*

Sarveswaran Ganesamoorthy − *Materials Science Group, IGCAR, Kalpakkam 603102, India; Homi Bhabha National Institute, Mumbai 400094, India*

Narayanasamy Vijayan − *CSIR-National Physical Laboratory, In-House BND Group, New Delhi 110012, India*

Godavarthi Bhagavannarayana − *VSM Group of Institutions, Ramachandrapuram, Andhra Pradesh 533255, India*

Ashwini Kumar Karnal − *Crystal Growth and Instrumentation Section, Laser and Functional Materials Division, Raja Ramanna Centre for Advanced Technology, Indore 452013, India; Homi Bhabha National Institute, Mumbai 400094, India*

Complete contact information is available at: https://pubs.acs.org/10.1021/acsomega.1c00452

Notes

The authors declare no competing financial interest.

ACKNOWLEDGMENTS

M.K.R.R. wishes to acknowledge the University Grants Commission (UGC) for the UGC-Non NET fellowship. Authors sincerely thank Prof M. A. Wahab, former Head, Department of Physics, Jamia Millia Islamia, for his suggestion during the experimental activities.

REFERENCES

(1) Kösters, M.; Sturman, B.; Werheit, P.; Haertle, D.; Buse, K. Optical cleaning of congruent lithium niobate crystals. *Nat. Photonics* **2009**, *3*, 510−513.

(2) Imlau, M.; Badorreck, H.; Merschjann, C. Optical nonlinearities of small polarons in lithium niobate. *Appl. Phys. Rev.* **2015**, *2*, No. 040606.

(3) Guarino, A.; Poberaj, G.; Rezzonico, D.; Degl'Innocenti, R.; Günter, P. Electro−optically tunable microring resonators in lithium niobate. *Nat. Photonics* **2007**, *1*, 407−410.

(4) Arizmendi, L. Photonic applications of lithium niobate crystals. *Phys. Status Solidi (a)* **2004**, *201*, 253−283.

(5) Ballman, A. A. Growth of piezoelectric and ferroelectric materials by the CzochraIski technique. *J. Am. Ceram. Soc.* **1965**, *48*, 112−113.

(6) Riscob, B.; Bhaumik, I.; Ganesamoorthy, S.; Bhatt, R.; Vijayan, N.; Karnal, A. K.; Wahab, M. A.; Bhagavannarayana, G. Effect of Mg doping on the growth aspects, crystalline perfection, and optical and thermal properties of congruent $LiNbO_3$ single crystals. *J. Appl. Crystallogr.* **2013**, *46*, 1854−1862.

(7) Shang, J.; Sun, J.; Li, Q.; Yang, J.; Zhang, L.; Xu, J. Single-block pulse-on electro-optic Q-switch made of $LiNbO_3$. *Sci. Rep.* **2017**, *7*, 4651.

(8) Werner, C. S.; Herr, S. J.; Buse, K.; Sturman, B.; Soergel, E.; Razzaghi, C.; Breunig, I. Large and accessible conductivity of charged domain walls in lithium niobate. *Sci. Rep.* **2017**, *7*, 9862.

(9) Carruthers, J. R.; Peterson, G. E.; Grasso, M.; Bridenbaugh, P. M. Nonstoichiometry and crystal growth of lithium niobate. *J. Appl. Phys.* **1971**, *42*, 1846−1851.

(10) Kitamura, K.; Yamamoto, J. K.; Iyi, N.; Kirnura, S.; Hayashi, T. Stoichiometric $LiNbO_3$ single crystal growth by double crucible

Czochralski method using automatic powder supply system. *J. Cryst. Growth* **1992**, *116*, 327−332.
(11) Iyi, N.; Kitamura, K.; Izumi, F.; Yamamoto, J. K.; Hayashi, T.; Asano, H.; Kimura, S. Comparative study of defect structures in lithium niobate with different compositions. *J. Solid State Chem.* **1992**, *101*, 340−352.
(12) Riscob, B.; Bhatt, R.; Vijayan, N.; Bhaumik, I.; Ganesamoorthy, S.; Wahab, M. A.; Rashmi; Bhagavannarayana, G. Structural, optical and thermal properties of Zr−Fe co-doped congruent $LiNbO_3$ single crystals. *J. Appl. Crystallogr.* **2013**, *46*, 601−609.
(13) Qiao, H.; Xu, J.; Zhang, G.; Zhang, X.; Sun, Q.; Zhang, G. Ultraviolet photorefractivity features in doped lithium niobate crystals. *Phys. Rev. B* **2004**, *70*, No. 094101.
(14) Volk, T.; Wöhlecke, M.; Rubinina, N.; Razumovski, N. V.; Jermann, F.; Fischer, C.; Böwer, R. $LiNbO_3$ with the damage-resistant impurity indium. *Appl. Phys. A: Mater. Sci. Process.* **1995**, *60*, 217−225.
(15) Zhong, G.; Jin, J.; Wu, Z. *Proceedings of 11th International Quantum Electronic Conference: IEEE*, Cat. No. 80 CH1S61−0, p. 631. Washington, DC, Optical Society of America. 1980
(16) Bryan, D. A.; Gerson, R.; Tomaschke, H. E. Increased optical damage resistance in lithium niobate. *Appl. Phys. Lett.* **1984**, *44*, 847−849.
(17) Furukawa, Y.; Sato, M.; Nitanda, F.; Ito, K. Growth and characterization of MgO-doped $LiNbO_3$ for electro-optic devices. *J. Cryst. Growth* **1990**, *99*, 832−836.
(18) Grabmaier, B. C.; Otto, F. Growth and investigation of MgO-doped LiNbO3. *J. Cryst. Growth* **1986**, *79*, 682−688.
(19) Bhaumik, I.; Ganesamoorthy, S.; Bhatt, R.; Karnal, A. K.; Wadhawan, V. K.; Gupta, P. K.; Kitamura, K.; Takekawa, S.; Nakamura, M. The ferroelectric phase transition in lithium tantalate single crystals: A composition-dependence study. *J. Appl. Phys.* **2008**, *103*, No. 014108.
(20) Iyi, N.; Kitamura, K.; Yajima, Y.; Kimura, S.; Furukawa, Y.; Sato, M. Defect structure model of MgO-doped LiNbO3. *J. Solid State Chem.* **1995**, *118*, 148−152.
(21) Liu, J.; Zhang, W.; Zhang, G. Defect chemistry analysis of the defect structure in Mg-doped $LiNbO_3$ crystals. *Phys. Status Solidi (a)* **1996**, *156*, 285−291.
(22) Schlarb, U.; Betzler, K. Influence of the defect structure on the refractive indices of undoped and Mg-doped lithium niobate. *Phys. Rev. B* **1994**, *50*, 751−757.
(23) Ishizuki, H.; Shoji, I.; Taira, T. High-energy quasi-phase-matched optical parametric oscillation in a 3-mm-thick periodically poled MgO: $LiNbO_3$ device. *Opt. Lett.* **2004**, *29*, 2527−2529.
(24) Zhang, J.; Chen, Y.; Lu, F.; Chen, X. Flexible wavelength conversion via cascaded second order nonlinearity using broadband SHG in MgO-doped PPLN. *Opt. Express* **2008**, *16*, 6957−6962.
(25) Bhatt, R.; Bhaumik, I.; Ganesamoorthy, S.; Bright, R.; Soharab, M.; Karnal, A.; Gupta, P. Control of intrinsic defects in lithium niobate single crystal for optoelectronic applications. *Crystals* **2017**, *7*, 23.
(26) Rahman, M. K. R.; Riscob, B.; Singh, B.; Bhatt, R.; Bhaumik, I.; Ganesamoorthy, S.; Vijayan, N.; Karnal, A. K.; Bdikin, I.; Nair, L. Nanoindentation and structural studies of MgO-doped congruent $LiNbO_3$ single crystals. *Mater. Chem. Phys.* **2021**, *264*, 124425.
(27) Ramaz, F.; Rakitina, L.; Gospodinov, M.; Briat, B. Photo-refractive and photochromic properties of ruthenium-doped $Bi_{12}SiO_{20}$. *Opt. Mater.* **2005**, *27*, 1547−1559.
(28) Riscob, B.; Bhaumik, I.; Ganesamoorthy, S.; Bhatt, R.; Vijayan, N.; Zimik, K.; Karnal, A. K.; Bhagavannarayana, G.; Gupta, P. K. Crystal growth of Ru-doped congruent $LiNbO_3$ and investigation of crystalline perfection and optical properties. *J. Appl. Crystallogr.* **2015**, *48*, 1753−1760.
(29) Marinova, V.; Lin, S. H.; Hsu, K. Y.; Hsieh, M.-L.; Gospodinov, M. M.; Sainov, V. Optical and holographic properties of $Bi_4Ge_3O_{12}$ crystals doped with ruthenium. *J. Mater. Sci.: Mater. Electron.* **2003**, *14*, 857−858.
(30) Fujimura, R.; Kubota, E.; Matoba, O.; Shimura, T.; Kuroda, K. Photorefractive and photochromic properties of Ru doped $Sr_{0.61}Ba_{0.39}Nb_2O_6$ crystal. *Opt. Commun.* **2002**, *213*, 373−378.
(31) Marinova, V.; Hsieh, M.-L.; Lin, S. H.; Hsu, K. Y. Effect of ruthenium doping on the optical and photorefractive properties of $Bi_{12}TiO_{20}$ single crystals. *Opt. Commun.* **2002**, *203*, 377−384.
(32) Chiang, C. H.; Chen, J. C. Growth and properties of Ru-doped lithium niobate crystal. *J. Cryst. Growth* **2006**, *294*, 323−329.
(33) Bhatt, R.; Bhaumik, I.; Ganesamoorthy, S.; Karnal, A. K.; Gupta, P. K.; Swami, M. K.; Patel, H. S.; Sinha, A. K.; Upadhyay, A. Study of structural defects and crystalline perfection of near stoichiometric $LiNbO_3$ crystals grown from flux and prepared by VTE technique. *J. Mol. Struct.* **2014**, *1075*, 377−383.
(34) Lal, K.; Bhagavannarayana, G. A high-resolution diffuse X-ray scattering study of defects in dislocation-free silicon crystals grown by the float-zone method and comparison with Czochralski-grown crystals. *J. Appl. Crystallogr.* **1989**, *22*, 209−215.
(35) Bhagavannarayana, G.; Kushwaha, S. K. Enhancement of SHG efficiency by urea doping in ZTS single crystals and its correlation with crystalline perfection as revealed by Kurtz powder and high-resolution X-ray diffraction methods. *J. Appl. Crystallogr.* **2010**, *43*, 154−162.
(36) Senthil Kumar, K.; Moorthy Babu, S.; Bhagavannarayana, G. Study of the influence of dopants on the crystalline perfection of ferroelectric glycine phosphite single crystals using high-resolution X-ray diffraction analysis. *J. Appl. Crystallogr.* **2011**, *44*, 313−318.
(37) Bhaumik, I.; Bhatt, R.; Ganesamoorthy, S.; Saxena, A.; Karnal, A. K.; Gupta, P. K.; Sinha, A. K.; Deb, S. K. Temperature-dependent index of refraction of monoclinic Ga_2O_3 single crystal. *Appl. Opt.* **2011**, *50*, 6006−6010.
(38) Kurtz, S. K.; Perry, T. T. A powder technique for the evaluation of nonlinear optical materials. *J. Appl. Phys.* **1968**, *39*, 3798−3813.
(39) Bhagavannarayana, G.; Ananthamurthy, R. V.; Budakoti, G. C.; Kumar, B.; Bartwal, K. S. A study of the effect of annealing on Fe-doped $LiNbO_3$ by HRXRD, XRT and FT−IR. *J. Appl. Crystallogr.* **2005**, *38*, 768−771.
(40) Kushwaha, S. K.; Maurya, K. K.; Vijayan, N.; Kumar, B.; Bhatt, R.; Ganesamoorthy, S.; Bhagavannarayana, G. Crystalline perfection, Raman, UV-VIS-NIR and prism coupler investigations on Cz-grown pure and Zn-doped $LiNbO_3$ single crystals. *CrystEngComm* **2012**, *14*, 3297−3305.
(41) Batterman, B. W.; Cole, H. Dynamical diffraction of X rays by perfect crystals. *Rev. Mod. Phys.* **1964**, *36*, 681−717.
(42) Kushwaha, S. K.; Maurya, K. K.; Vijayan, N.; Bhagavannarayana, G. Crystalline perfection, EPR, prism coupler and UV-VIS-NIR studies on Cz-grown Fe-doped $LiNbO_3$: A photorefractive nonlinear optical crystal. *CrystEngComm* **2011**, *13*, 4866−4872.
(43) Bhatt, R.; Ganesamoorthy, S.; Bhaumik, I.; Karnal, A. K.; Bhagavannarayana, G.; Gupta, P. K. Effect of annealing in Li-rich ambient on the optical absorption and crystallinity of Er doped $LiNbO_3$ crystals. *J. Optoelectron. Adv. Mater.* **2011**, *13*, 245−250.
(44) Bhagavannarayana, G.; Parthiban, S.; Meenakshisundaram, S. An interesting correlation between crystalline perfection and second harmonic generation efficiency on KCl- and oxalic acid-doped ADP crystals. *Cryst. Growth Des.* **2008**, *8*, 446−451.
(45) Sidorov, N. V.; Palatnikov, M. N.; Gabrielyan, V. T.; Chufyrev, P. G.; Kalinnikov, V. T. Raman spectra and structural perfection of nominally pure lithium niobate crystals. *Inorg. Mater.* **2007**, *43*, 60−67.
(46) Hermet, P.; Veithen, M.; Ghosez, P. First-principles calculations of the nonlinear optical susceptibilities and Raman scattering spectra of lithium niobate. *J. Phys.: Condens. Matter* **2007**, *19*, 456202.
(47) Caciuc, V.; Postnikov, A. V.; Borstel, G. Ab initio structure and zone-center phonons in $LiNbO_3$. *Phys. Rev. B* **2000**, *61*, 8806−8813.
(48) Schlarb, U.; Klauer, S.; Wesselmann, M.; Betzler, K.; Wöhlecke, M. Determination of the Li/Nb ratio in lithium niobate by means of

https://doi.org/10.1021/acsomega.1c00452
ACS Omega 2021, 6, 10807−10815

birefringence and Raman measurements. *Appl. Phys. A: Mater. Sci. Process.* **1993**, *56*, 311−315.
(49) Bhatt, R.; Ganesamoorthy, S.; Bhaumik, I.; Karnal, A. K.; Wadhawan, V. K. Growth rate anisotropy and absorption studies on β-BaB_2O_4 single crystals grown by the top-seeded solution growth technique. *Opt. Mater.* **2007**, *29*, 801−805.
(50) Aleksandrovskiĭ, A. L.; Ershova, G. I.; Kitaeva, G. K.; Kulik, S. P.; Naumova, I. I.; Tarasenko, V. V. Dispersion of the refractive indices of $LiNbO_3$:Mg and $LiNbO_3$:Y crystals. *Quantum Electron.* **1991**, *21*, 225.
(51) Kovács, L.; Ruschhaupt, G.; Polgár, K.; Corradi, G.; Wöhlecke, M. Composition dependence of the ultraviolet absorption edge in lithium niobate. *Appl. Phys. Lett.* **1997**, *70*, 2801−2803.
(52) Bhatt, R.; Ganesamoorthy, S.; Bhaumik, I.; Karnal, A. K.; Gupta, P. K. Optical bandgap and electrical conductivity studies on near stoichiometric $LiNbO_3$ crystals prepared by VTE process. *J. Phys. Chem. Solids* **2012**, *73*, 257−261.
(53) Chiang, C. H.; Chen, J. C.; Lee, Y. C.; Lin, C. H.; Chang, J. Y. Photorefractive properties of Ru doped lithium niobate crystal. *Opt. Mater.* **2009**, *31*, 812−816.
(54) Tauc, J. C. *Optical properties of solids*, (North -Holland: Amsterdam). 1972, p372
(55) Bhatt, R.; Bhaumik, I.; Ganesamoorthy, S.; Karnal, A. K.; Swami, M. K.; Patel, H. S.; Gupta, P. K. Urbach tail and bandgap analysis in near stoichiometric LiNbO3 crystals. *Phys. Status Solidi (a)* **2012**, *209*, 176−180.
(56) Urbach, F. The long-wavelength edge of photographic sensitivity and of the electronic absorption of solids. *Phys. Rev.* **1953**, *92*, 1324.
(57) Wemple, S. H.; DiDomenico, M., Jr. Oxygen-Octahedra Ferroelectrics. II. Electro-optical and Nonlinear-Optical Device Applications. *J. Appl. Phys.* **1969**, *40*, 735−752.
(58) Bhatt, R.; Kar, S.; Bartwal, K. S.; Shula, V.; Sen, P.; Sen, P. K.; Wadhawan, V. K. Studies on nonlinear optical properties of ferroelectric MgO-$LiNbO_3$ single crystals. *Ferroelectrics* **2005**, *323*, 165−169.

https://doi.org/10.1021/acsomega.1c00452
ACS Omega 2021, 6, 10807−10815